

Optical symmetries and anisotropic transport in high- T_c superconductors

T.P. Devereaux

Department of Physics, University of Waterloo, Waterloo, ON, N2L 3G1, Canada

(Dated: February 7, 2020)

A simple symmetry analysis of in-plane and out-of-plane transport in a family of high temperature superconductors is presented. It is shown that generalized scaling relations exist between the low frequency electronic Raman response and the in-plane and out-of-plane DC conductivities in both the normal and superconducting states of the cuprates. Specifically, for both the normal and superconducting state, the temperature dependence of the low frequency B_{1g} Raman slope scales with the c -axis dc conductivity, while the B_{2g} Raman slope scales with the in-plane dc conductivity. Comparison with experiments in the normal state of Bi-2212 and Y-123 imply that the nodal transport is largely doping independent and metallic, while transport near the BZ axes is governed by a quantum critical point near optimal doping. Important differences for La-214 are discussed. It is also shown that the c -axis conductivity rise for $T \ll T_c$ is a consequence of partial conservation of in-plane momentum for out-of-plane transport.

PACS numbers: 74.25.Jb, 71.27.+a, 78.30.-j

I. INTRODUCTION

The strong anisotropy of in-plane (ab) and out-of-plane (c) transport in the cuprate systems as probed by angle-resolved photoemission spectroscopy (ARPES), NMR rates, Raman experiments as well as Hall probes, resistivity, and optical conductivity is as unresolved and long-standing a problem as superconductivity itself^{1,2,3,4,5,6}. As a function of hole doping per CuO_2 plaquette p the ab -plane resistivity $\rho_{ab}(T)$ (Fig. 1A) shows a metallic temperature dependence ($d\rho/dT > 0$) for all p while the c -axis resistivity $\rho_c(T)$ (Fig. 1B) varies as T^r with an exponent r that changes from 2 to -2 as p decreases^{1,2,3,4,5,6}. The resistivity ratio $\rho_c(T)/\rho_{ab}(T)$ is large and becomes increasingly temperature dependent in all (hole-doped) cuprate systems for p below $\simeq 0.22$ at low temperatures.

It was pointed out early on that the c -axis properties provided an useful spectral tool to examine in-plane charge dynamics⁷. As a result, many approaches have been put forward to address the nature of in-plane versus out-of-plane transport^{7,8,9,10,11,12,13,14,15,16,17,18,19} in terms of anisotropy of the in-plane quasiparticle (qp) self energies $\Sigma(\mathbf{k}, T)$ and c -axis hopping $t_{\perp}(\mathbf{k})$, respectively, impurity assisted hopping, interband transitions, or in terms of “confinement-deconfinement” of electrons. Recently the issue of relating spectral weight in optical conductivity measurements to energy changes brought about by superconductivity has attracted a great deal of attention^{6,7,8}. The mechanism by which truly 3D superconducting coherence sets in is of continued interest and debate which has been guided in a large part by the measurements of the c -axis transport properties.

The issue is still largely unsettled basically due to the open question of whether electron hopping in the out-of-plane direction is coherent^{5,6,7,8,9}. If there were an at least partial conservation of the in-plane momentum for qp tunnelling along the c -axis, LDA²⁰ would indeed predict an interrelation between c -axis transport and the qp scattering rate close to $(\pi, 0)$ in the Brillouin zone (BZ).

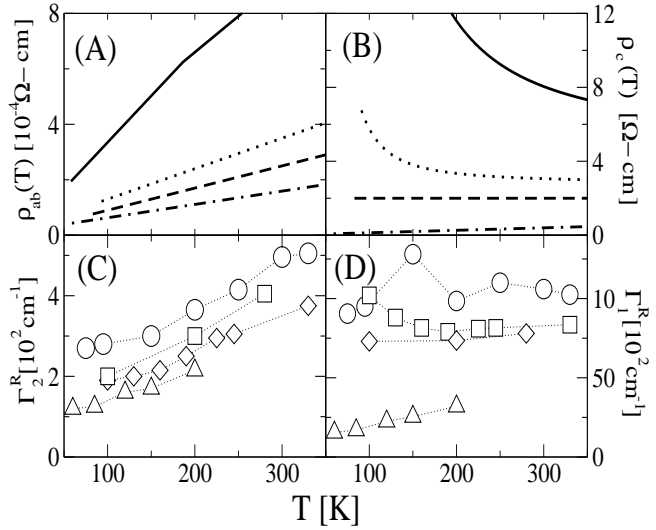


FIG. 1: Experimental results for Bi-2212 for $\rho_{ab}(T)$ (Panel A), $\rho_c(T)$ (Panel B), the Raman-derived B_{2g} , B_{1g} qp relaxation rate $\Gamma_{2,1}^R$ (Panel C, Panel D), respectively. The solid lines, circles correspond to underdoped samples ($p = 0.10$) with $T_c \sim 57\text{K}$, dotted lines, squares correspond to optimally doped samples ($p = 0.15$) with $T_c \sim 92\text{K}$, dashed lines, diamonds correspond to slightly overdoped samples ($p = 0.19$) with $T_c \sim 82\text{K}$, and the dotted-dashed lines, triangles correspond to overdoped samples ($p = 0.23$) with $T_c \sim 52\text{K}$. All resistivities were measured in Ref.³, except for the overdoped ($T_c = 52\text{K}$) sample which was measured in Ref.⁴. The Raman qp relaxation rates are taken from Ref.²¹.

What would be extremely useful would be a transport measurement beside conductivity which might directly test whether transport in the plane is intimately tied to out-of-plane transport.

A behavior similar to the resistivity anisotropy is reflected in electronic Raman scattering measurements when comparing the temperature dependence of the low energy continuum measured in B_{1g} polarization orient-

tations, which project out charge fluctuations near the BZ axes, to B_{2g} configurations, which probe charge fluctuations along the BZ diagonals. Refs.²¹ and²² compared the Raman relaxation rate in each channel, defined as the inverse of the slope of the low energy Raman response $\Gamma_{1,2}^R = \lim_{\Omega \rightarrow 0} [\partial \chi''_{\gamma,\gamma}(\Omega, T) / \partial \Omega]^{-1}$. For both $\text{YBa}_2\text{Cu}_3\text{O}_{7-\delta}$ (Y-123) and $\text{Bi}_2\text{Sr}_2\text{CaCu}_2\text{O}_{8+\delta}$ (Bi-2212), it was found that for B_{2g} symmetry, Γ_2^R (Fig. 1C) approximately scales with $\rho_{ab}(T)$ over the entire doping range, while for B_{1g} , Γ_1^R (Fig. 1D) was found to cross over from metallic to insulator behavior for p less than ~ 0.22 . This has recently been interpreted as evidence for an underlying quantum critical point lying near $p_c \simeq 0.22$ of an unconventional metal-insulator transition²².

In the superconducting state, the temperature dependence of the ab -plane dc conductivity^{23,24} typically shows a peak around $35K$ which is material dependent and has been attributed to the rapid collapse of the quasiparticle (qp) inelastic scattering rate below T_c and the small rise of the qp elastic scattering rate for low T .^{25,26,27,28} A similar peak seen in in-plane thermal conductivity measurements was found to be sensitive to annealing conditions²⁹. The c -axis dc conductivity in $\text{YBa}_2\text{Cu}_3\text{O}_{6.95}$ meanwhile does not show a peak in this region but has an upturn at temperatures below $20K$. The origin of the peak is currently not understood^{12,30}. The c -axis thermal conductivity was found to show a very weak peak which was again affected by annealing conditions²⁹. Much less is known about the temperature dependence of Raman scattering in the static limit in the superconducting state, although some theoretical treatments have appeared^{31,32}. In particular one would like to test whether features shown in conductivity measurements are found in Raman scattering measurements.

Shastry and Shraiman have noted the close similarity between the conductivity and the Raman response and have suggested a scaling relation exists between the two which follow the same temperature and frequency dependence³³:

$$\Omega \sigma'(\Omega, T) = \chi''(\Omega, T). \quad (1)$$

This Shastry-Shraiman (SS) relation holds if the qp scattering rate Γ and qp residue Z are independent of \mathbf{k} and has been shown to be exact for both the Hubbard and Falicov-Kimball models in the limit of large dimensions where the self energy and vertex corrections are local³⁴. Generally though any \mathbf{k} -dependence of Z and/or Γ invalidates the SS scaling relation making it inappropriate for strongly anisotropic systems such as the cuprates.

However, an approximate scaling relation may hold for certain cases and one purpose of this paper is to point out some of the connections between the conductivity and Raman response for strongly anisotropic systems and derive appropriate scaling relations. In particular we will, based on symmetry arguments, determine that a variant of the SS relation can be formulated to show that a scaling relation exists separately between σ_{ab} and $1/\Gamma_2^R$ and between σ_c and $1/\Gamma_1^R$ as a consequence of the momen-

tum dependence of $t_{\perp}(\mathbf{k})$, in-plane self energy $\Sigma(\mathbf{k})$, and a $d_{x^2-y^2}$ energy gap $\Delta(\mathbf{k})$. Comparison with the available data in the normal state suggests that qps located near the BZ axes or “hot spots” become gapped near optimal doping²² while the qps located along the BZ diagonals or “cold spots” are largely doping independent and remain metallic. Thus the c -axis transport is partially influenced by a correlation gap near $(\pi, 0)$ because of partial conservation of the in-plane momentum in c -axis transport and not completely by c -axis tunneling or diffusion. These scaling relations are found to also hold in the superconducting state and comparison with the available data imply that there exists well-defined qps for all regions of the BZ in contrast to the normal state. Various models for qp scattering as a function of doping are discussed, and it is found that generally no single model can adequately capture the complex nature of electron dynamics over a wide range of doping. Features of the theory in the superconducting state qualitatively describe the behavior seen in the c -axis conductivity, but there are important questions left unanswered. In conclusion, experimental evidence in both the normal and superconducting states suggest that the in-plane momentum is at least partially conserved in c -axis transport over a very wide doping range.

The plan of the paper is as follows: Sections II and III present the formalism used and the results for the temperature dependence of the in-plane and out-of-plane DC conductivity and low frequency Raman response in the normal and superconducting states, respectively, for the common model where t_{\perp} vanishes along the BZ diagonals, summarized in the Appendix. The results are summarized and open points are discussed in Section IV.

II. NORMAL STATE

The quantum chemistry of the tetragonal Cu-O system yields an out-of-plane hopping which is modulated by the in-plane momentum in such a way that it is strongly governed by qps located along the BZ axes as opposed to qps along the zone diagonal, $t_{\perp}(\mathbf{k}) = t_{\perp}^0 [\cos(k_x a) - \cos(k_y a)]^2$, as reviewed in the Appendix. This form for the hopping has been widely used to study the penetration depth¹¹, c -axis conductivity^{6,12,13}, and bi-layer splitting²⁰ in ARPES³⁶. However we note that inclusion of the Cu-O chains or O displacements would lower the symmetry with the consequence that the out-of-plane hopping would no longer vanish along the BZ diagonals which could only be noticeable at very low temperatures. We now explore the consequences of such a term on the dc conductivities and the symmetry-dependent electronic Raman response for qp scattering in the $a - b$ plane and along the c -axis in the following sections.

In linear response theory, expressions for the regular part of the conductivity and Raman response in the absence of vertex corrections are given as (here and

throughout we set $k_B = \hbar = 1$)

$$\begin{pmatrix} \Omega\sigma'_{\alpha,\beta}(\Omega) \\ \chi''_{\gamma,\gamma}(\Omega) \end{pmatrix} = \int \frac{dx}{\pi} [f(x) - f(x + \Omega)] \quad (2)$$

$$\times \sum_{\mathbf{k}} \begin{pmatrix} j_{\mathbf{k}}^{\alpha} j_{\mathbf{k}}^{\beta} \\ \gamma_{\mathbf{k}}^2 \end{pmatrix} G_{\mathbf{k}}^R(x) G_{\mathbf{k}}^A(x + \Omega),$$

Here f is the Fermi function, $j_{\mathbf{k}}^{\alpha} = e^{\frac{\partial \epsilon_{\mathbf{k}}}{\partial k_{\alpha}}}$ is the current vertex for direction α given in terms of the band dispersion $\epsilon_{\mathbf{k}}$ and electron charge e , and $\gamma_{\mathbf{k}}$ is the Raman vertex being set by choosing the incoming and outgoing light polarization vectors. Vertex corrections³⁷, which are certainly crucial for satisfying Ward identities for the calculation of the conductivity and particle number conservation for the pure charge channel, add an additional source of momentum and temperature dependence which has been explored in a spin-fermion model³⁸. However, they are nevertheless neglected since we are interested in exploring simple symmetry properties of the various experimental probes.

The current vertices are simply $j_{\mathbf{k}}^x = v_x \sin(k_x a)$, and $j_{\mathbf{k}}^z = v_z [\cos(k_x a) - \cos(k_y a)]^2$, where $v_x \sim t$ and $v_z \sim t_{\perp}^0$ have only a mild momentum dependence. In the limit where the incident and scattered photon energies are small compared to the bandwidth the Raman vertex is given as the curvature of the band: $\gamma_{\alpha,\beta} = \frac{\partial^2 \epsilon(\mathbf{k})}{\partial k_{\alpha} \partial k_{\beta}}$ ³⁹. The vertices are thus determined from the above band structure as $\gamma_{\mathbf{k}} = b_1 [\cos(k_x a) - \cos(k_y a)]$ for B_{1g} orientations, and $= b_2 \sin(k_x a) \sin(k_y a)$ for B_{2g} orientations, while for c -axis A_{1g} Raman $\gamma_{\mathbf{k}} = a_{zz} \cos(k_z c) [\cos(k_x a) - \cos(k_y a)]^2$. The prefactors $b_1 \sim t$, $b_2 \sim t'$, and $a_{zz} \sim t_{\perp}^0$ can be assumed to be only mildly frequency dependent corresponding to the experimentally observed off-resonant scattering and therefore are only multiplicative constants. Since the energy range considered is very small in comparison to all electronic bandwidths involved the assumption $b_{1,2}$ and a_{zz} to be constant is robust under all realistic circumstances.

As can be seen by the weighting of the vertices, we may expect similar behavior for the B_{2g} Raman and in-plane conductivity, and the B_{1g} , c -axis A_{1g} Raman, and the out-of-plane conductivity as well. The former two quantities assign weight around the Fermi surface (FS) to the diagonals while the latter three assign weight along the zone axes.

We begin by considering electron scattering as modelled by a phenomenological momentum, frequency, and temperature dependent self energy resulting from the exchange of an (undetermined) intermediate boson: $G_{\mathbf{k}}^{R,A}(\omega) = Z_{\mathbf{k}}(\omega, T)/(\omega - \bar{\epsilon}_{\mathbf{k}} \pm i\Gamma_{\mathbf{k}}(\omega, T)) + G_{inc}$. Here $\bar{\epsilon}$ is the renormalized band structure, $Z_{\mathbf{k}}(\omega, T) = [1 - \partial \Sigma'_{\mathbf{k}}(\omega, T)/\partial \omega]^{-1}$ is the qp residue, and $\Gamma_{\mathbf{k}}(\omega, T)$ is the momentum, frequency, and temperature dependent qp scattering rate. At this point we neglect and singularities or near singularities of the self energy indicative of an incipient phase transition and thus restrict consideration to metallic phases.

Converting the momentum sum to an integral over an infinite band plus an average over the FS and neglecting the incoherent part G_{inc} , we obtain in the limit of low frequencies

$$\begin{pmatrix} \sigma'_{\alpha,\beta}(\Omega \rightarrow 0, T) \\ \partial \chi''_{\gamma,\gamma}(\Omega \rightarrow 0, T)/\partial \Omega \end{pmatrix} = -2N_F \int dx \frac{\partial f(x)}{\partial x} \times \left\langle \begin{pmatrix} j_{\mathbf{k}}^{\alpha} j_{\mathbf{k}}^{\beta} \\ \gamma_{\mathbf{k}}^2 \end{pmatrix} \frac{Z_{\mathbf{k}}^2(x, T) \Gamma_{\mathbf{k}}(x, T)}{\Omega^2 + [2\Gamma_{\mathbf{k}}(x, T)]^2} \right\rangle, \quad (3)$$

where $\langle \dots \rangle$ denote performing an average over the FS. In what follows we neglect specific features of and off the FS (such as van Hove) and approximate the 2D FS as a circle and expand the c -axis dispersion for small t_{\perp}^0 to obtain:

$$\begin{aligned} xx \text{ Conductivity, } & j^x = v_F \sin(\phi), \\ zz \text{ Conductivity, } & j^z = v_z \cos^2(2\phi), \\ B_{1g} \text{ Raman, } & \gamma_{B_{1g}} = b_1 \cos(2\phi), \\ B_{2g} \text{ Raman, } & \gamma_{B_{2g}} = b_2 \sin(2\phi), \\ zz \text{ } A_{1g} \text{ Raman, } & \gamma_{A_{1g,zz}} = a_{zz} \cos^2(2\phi) \end{aligned} \quad (4)$$

Moreover we note that the c -axis conductivity and $\partial \chi''_{zz}/\partial \Omega$ are given by the same expressions, in accordance with the qp scattering rate not having a k_z dependence. Therefore we confirm the SS relation for the out-of-plane A_{1g} Raman and conductivity, respectively, and in what follows we drop discussion of the out-of-plane A_{1g} Raman.

We now focus on the low frequency response (static or dc limit) to connect the IR and Raman to transport and ARPES. In the static limit at low temperatures we find from Eq. 3

$$\begin{pmatrix} \sigma'_{\alpha,\beta}(T) \\ \partial \chi''_{\gamma,\gamma}(T)/\partial \Omega \end{pmatrix} = N_F \left\langle \begin{pmatrix} j_{\mathbf{k}}^{\alpha} j_{\mathbf{k}}^{\beta} \\ \gamma_{\mathbf{k}}^2 \end{pmatrix} \frac{Z_{\mathbf{k}}^2(T)}{2\Gamma_{\mathbf{k}}(T)} \right\rangle. \quad (5)$$

The static limits thus show the interplay of the anisotropies of the scattering rate and the vertices governing the response functions.

The simple expression for the static limits allows for a straightforward comparison of models for the qp scattering rate. We choose a generic model which describes scattering weighted largely along the BZ axes plus a temperature dependent scattering rate taken to be uniform around the FS:

$$\Gamma_{\mathbf{k}}(T) = \Gamma_h(T) \cos^2(2\phi) + \Gamma_c(T). \quad (6)$$

This form for the qp scattering rate has been widely employed in a number of models differing in the representations of Γ_h and Γ_c ^{14,15,16,17} constrained only to possess the full symmetry of the lattice (A_{1g}). Further parameterizations of the anisotropy do not lead to appreciable differences. For the B_{2g} Raman as well as the in-plane conductivity, the vertices weight out regions of the FS where the scattering rate is small, along the FS diagonals

or “cold spots”. However, the B_{1g} and c -axis A_{1g} Raman and the out-of-plane conductivity assign no weight to the diagonals and thus will be governed by the scattering at the “hot spots”.

Neglecting the \mathbf{k} -dependence of the qp residue, the resulting integrals can be easily performed to give

$$\sigma'_{xx}(T) = v_F^2 \frac{N_F Z^2}{2\Gamma_c(T)} \frac{1}{\sqrt{1 + \Gamma_h(T)/\Gamma_c(T)}}, \quad (7)$$

$$\begin{aligned} \sigma'_{zz}(T) = v_z^2 \frac{N_F Z^2}{2\Gamma_h(T)} & \left\{ \frac{1}{2} - \frac{\Gamma_c(T)}{\Gamma_h(T)} \right. \\ & \left. \times \left(1 - \frac{1}{\sqrt{1 + \Gamma_h(T)/\Gamma_c(T)}} \right) \right\}, \end{aligned} \quad (8)$$

$$\begin{aligned} \frac{\partial \chi''_{B_{1g}}(T)}{\partial \Omega} = b_1^2 \frac{N_F Z^2}{2\Gamma_h(T)} & \\ & \times \left\{ 1 - \frac{1}{\sqrt{1 + \Gamma_h(T)/\Gamma_c(T)}} \right\}, \end{aligned} \quad (9)$$

$$\begin{aligned} \frac{\partial \chi''_{B_{2g}}(T)}{\partial \Omega} = b_2^2 \frac{N_F Z^2}{2\Gamma_h(T)} & \frac{1}{\sqrt{1 + \Gamma_h(T)/\Gamma_c(T)}} \\ & \times \left\{ 1 - \sqrt{1 + \Gamma_h(T)/\Gamma_c(T)} + \right. \\ & \left. \Gamma_h(T)/\Gamma_c(T) \right\}. \end{aligned} \quad (10)$$

These results for the ab-plane and c -axis conductivity have been derived several times, most recently by Refs.^{12,13}. However here it can be seen that there is a direct connection between conductivities and Raman response functions. It is clear that the function form for the scattering rate determines the temperature dependence of all four response functions.

Early on, ARPES measurements³⁵ yielded $\Gamma_c \ll \Gamma_h$ from smeared spectral functions seen near the BZ axes compared to the BZ diagonals. However, recent ARPES measurements³⁶ indicated bi-layer splitting may have led to an overestimation of Γ_h , but still the limit $\Gamma_c \ll \Gamma_h$ is a useful limit to explore. In this limit the response functions are

$$\sigma'_{xx}(T) = v_F^2 \frac{N_F Z^2}{2\sqrt{\Gamma_c(T)\Gamma_h(T)}}, \quad (11)$$

$$\sigma'_{zz}(T) = v_z^2 \frac{N_F Z^2}{2\Gamma_h(T)}, \quad (12)$$

$$\frac{\partial \chi''_{B_{1g}}(T)}{\partial \Omega} = b_1^2 \frac{N_F Z^2}{2\Gamma_h(T)}, \quad (13)$$

$$\frac{\partial \chi''_{B_{2g}}(T)}{\partial \Omega} = b_2^2 \frac{N_F Z^2}{2\sqrt{\Gamma_h(T)\Gamma_c(T)}}. \quad (14)$$

This directly shows the similarity between the B_{1g} Raman slope and the c -axis conductivity, and B_{2g} Raman slope and the in-plane conductivity, regardless of the functional form chosen for two contributions to the qp scattering rate. Thus in this model consistent with

experiments, a variant of the SS relation for the cuprates may be expressed as

$$\begin{aligned} \lim_{\Omega \rightarrow 0} \Omega \sigma'_{xx}(T) &= \chi''_{B_{2g}}(\Omega, T), \\ \lim_{\Omega \rightarrow 0} \Omega \sigma'_{zz}(T) &= \chi''_{B_{1g}}(\Omega, T). \end{aligned} \quad (15)$$

This demonstrates how out-of-plane transport can be directly inferred from in-plane optical transport measurements. Further, this confirms the behavior shown in Fig. (1), indicating that the in-plane momentum must be at least partially conserved for transport perpendicular to the CuO_2 planes.

We now consider several models for $\Gamma_h(T)$ and $\Gamma_c(T)$. In both a “cold spot”¹⁴ and “hot spot” model¹⁵, $\Gamma_c(T)$ describes weakly renormalized qp scattering primarily along the FS diagonals generally of the form

$$\Gamma_c(T) = \Gamma_{imp} + T^2/T_0, \quad (16)$$

where Γ_{imp} represents elastic impurity scattering and T_0 is the energy scale of a renormalized Fermi liquid. The impurity scattering may be chosen to reproduce the extrapolated $T = 0$ resistivity and T_0 is a parameter to be chosen to fit a cross-over from T to T^2 in the resistivity. In the “hot spot” model, $\Gamma_h(T) = \sqrt{\Gamma_{hs}T}$ represents scattering with exchange of momentum \mathbf{Q} which has been employed in Ref.¹⁵ to determine the in-plane and Hall resistivity. In the “cold spot” model¹⁴, $\Gamma_h(T)$ is taken to be a constant Γ_{hs} presumed to arise from strong $d_{x^2-y^2}$ pairing fluctuations, and has been employed in several works to describe in-plane and out-of-plane optical conductivity and magneto-transport^{13,14,16}. In the marginal Fermi liquid (MFL) model most recently described in Ref.¹⁷, $\Gamma_c(T) \sim T$ and $\Gamma_h(T) \sim \text{constant}$ due to impurity scattering in correlated systems whereby strong correlation nearby a point-like scatterer induce real-space extensions of the impurity potential⁴⁰. In general, $\Gamma_h(T)$ and $\Gamma_c(T)$ are further constrained by the estimated width of the spectral function measured in ARPES experiments³⁶.

Following Ref.²¹, the “Raman scattering rate” $\Gamma_\mu^R(T)$ for each channel is defined as the inverse of the Raman slope $\Gamma_\mu^R(T) = \left[\frac{\partial \chi''_\mu(\Omega \rightarrow 0, T)}{\partial \Omega} \right]^{-1}$ as in Ref.²¹ in order to obtain information on the single particle scattering rate on regions of the FS selected by polarization orientations $\mu = 1, 2$ for $B_{1g, 2g}$, respectively. In the “hot spot model” we obtain $\Gamma_1^R \sim T^{1/2}$ and $\Gamma_2^R \sim T^{5/4}$, respectively, while in the “cold spot” model we obtain $\Gamma_1^R \sim \text{constant}$ and $\Gamma_2^R \sim T$, respectively. The MFL model yields $\Gamma_1^R \sim \text{constant}$ and $\Gamma_2^R \sim \sqrt{T}$, respectively. None of the models considered have presented analytic forms for the scattering rate as a function of doping, and presumably in all models the differences between Γ_h and Γ_c would be expected to vanish in overdoped systems.

It is often useful to look at the “scattering ratio” $\Gamma_1^R(T)/\Gamma_2^R(T) \sim \rho_c(T)/\rho_{ab}(T) \sim T^{-m}$. The models discussed give $m = 1/2, 3/4$, and 1 for MFL, “hot”, and “cold” spot models, respectively. These preceding exponents are summarized in Table I.

TABLE I: Summary of the low temperature dependence of the inverse conductivities, the Raman relaxation rates Γ_μ^R and the scattering ratio defined in the text.

Response	MFL	“Hot spot”	“Cold spot”
$\Gamma_2^R(T), \sigma_{xx}^{-1}(T)$	$T^{1/2}$	$T^{5/4}$	T
$\Gamma_1^R(T), \sigma_{zz}^{-1}(T)$	constant	$T^{1/2}$	constant
$\Gamma_1^R/\Gamma_2^R, \sigma_{xx}/\sigma_{zz}$	$T^{-1/2}$	$T^{-3/4}$	T^{-1}

The data for the Raman derived scattering ratio for Bi-2212 is shown in Fig. 2. The data are derived from the measurements shown in Fig. 1. The ratio derived from the measurements on three differently doped samples of Y-123 are shown in Fig. 3. For Bi-2212 the ratio slightly increases ($m < 0$) with temperature for appreciably overdoped systems, in agreement with the results obtained for $\text{La}_{2-x}\text{Sr}_x\text{CuO}_4$ (La-214)⁴¹. For decreasing doping p in both Bi-2212 and Y-123, the exponent m is positive and increases as the “hot” qps become gapped and the “cold” qps do not appreciably change. The large variation of the data from the underdoped Bi-2212 sample is due to the small intensity at low frequencies from which the slope is derived. Apart from this sample however a power-law fit adequately describes the data for both compounds. An exponential dependence on temperature has been used in Refs.³ for the resistivity ratio to determine the magnitude of a pseudogap, for example. The Raman ratios do not show enough exponential curvature to justify an extraction of a pseudogap temperature. The curvature may be obscured by the small signals measured at low frequencies however. Near optimum doping both the MFL and “cold spot” model give reasonable agreement for the “scattering ratio” while on the underdoped side the “cold spot” model gives an exponent of 1 in agreement with the data on Y-123 and in rough agreement with the data on Bi-2212.

It is important to point out that the results obtained on La-214 are qualitatively different from Y-123 and Bi-2212 in underdoped systems⁴¹. For $\text{La}_{1.9}\text{Sr}_{0.1}\text{CuO}_4$, a clear Fermi liquid like peak develops at low frequencies in the B_{1g} channel which sharpens as temperature is lowered so that $\partial\chi''(T)/d\Omega$ falls with decreasing temperature, similar to the behavior of the B_{2g} channel in Y-123 and Bi-2212. These features appear more or less continuously with doping. However, the peak in the B_{2g} channel seems to mimic the B_{2g} response in Y-123 and Bi-2212. The origin of this difference is unknown, but may be related to the presence of stripes such as those which occur in a nematic or smectic Fermi liquid⁴². If the stripes are considered conducting and statically aligned along the Cu-O bond directions, then B_{2g} would have a polarization component perpendicular to the stripes and would only measure incoherent excitations while B_{1g} would have a finite project of both the incident and scattering polarization light vectors along the stripes and would measure coherent, conducting excitations consistent with observations.

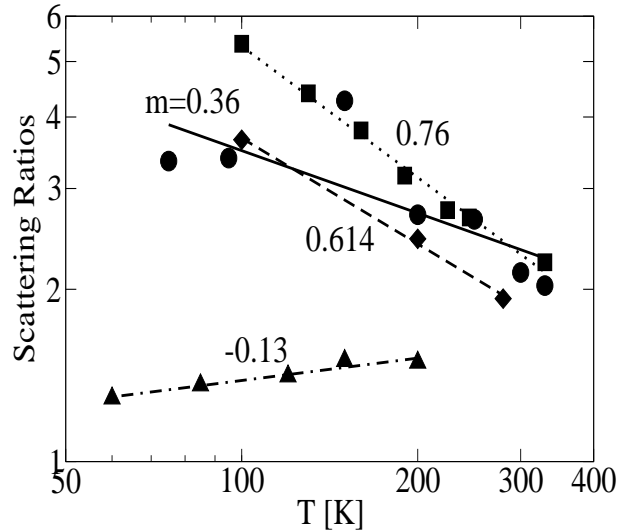


FIG. 2: A log-log plot of the Raman derived “scattering ratios” Γ_1^R/Γ_2^R (defined in the text) for Bi-2212 for underdoped (circles, $m = 0.36$), optimally doped (squares, $m = 0.76$), slightly overdoped (diamonds, $m = 0.614$) and appreciably overdoped (triangles, $m = -0.13$) samples shown in Fig. 1, respectively. The exponent m is determined from a least-squares fit to T^{-m} .

If the stripes were oriented 45° to the Cu-O directions or were considered to be non-conductive, then the roles of B_{1g} and B_{2g} would be reversed. Nevertheless, if the stripes were dynamically fluctuating, then simple symmetry considerations would have to be augmented and it is not clear whether on average light scattering would be sensitive to local stripe order. More data and further calculations are essentially needed to clarify this point. It is an important and open issue to understand why this occurs for a wide range of doping in La-214 and not Y-123 and Bi-2212.

The upturn of both $\Gamma_1(T)$ and $\rho_c(T)$ at low temperatures for underdoped systems is not captured by any model considered. Therefore in what follows the role of anisotropy in the qp residue Z is explored in a simple effort to model the effect of a loss of qp transport for the “hot” qps with decreasing p . This recently has been addressed regarding charge renormalizations⁴³. Taking $Z_{\mathbf{k}}(T) = Z_h e^{-(E_g/T) \cos^2(2\Phi)}$ as a phenomenological model of angular dependent gapping of qps with an energy scale E_g , the integrals are straightforward and the result can be expressed analytically in terms of a degenerate hypergeometric function of two variables:

$$\begin{aligned} \sigma'_{xx}(T), \partial\chi''_{B_{2g}}(T)/\partial\Omega &\sim \\ \sigma'_{zz}(T), \partial\chi''_{B_{1g}}(T)/\partial\Omega &\sim \\ \frac{N_F}{2\Gamma_c(T)} \begin{cases} \Phi_1\left(\frac{1}{2}, 1, 2, -\frac{\Gamma_h}{\Gamma_c(T)}, -\frac{T_{pg}}{T}\right), \\ \Phi_1\left(\frac{3}{2}, 1, 2, -\frac{\Gamma_h}{\Gamma_c(T)}, -\frac{T_{pg}}{T}\right). \end{cases} \end{aligned} \quad (17)$$

For almost all temperatures, the function can be ac-

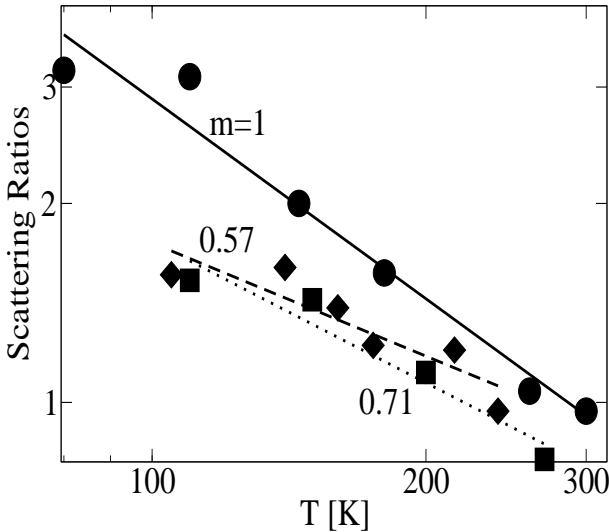


FIG. 3: A log-log plot of the data obtained in Ref.²¹ for the Raman derived “scattering ratios” Γ_1^R/Γ_2^R (defined in the text) for $\text{YBa}_2\text{Cu}_3\text{O}_{6.5}$ (circles, $m = 1$), $\text{YBa}_2\text{Cu}_3\text{O}_{6.93}$ (squares, $m = 0.71$), and $\text{YBa}_2\text{Cu}_3\text{O}_{6.98}$ (diamonds, $m = 0.57$), respectively.

curately described as the previous results Eqs. (11–14) with the sole exception that $\sigma'_{zz}(T)$ Eq. (12) and $\partial\chi''_{B_{1g}}(T)/\partial\Omega$ Eq. (14) are multiplied by $e^{2E_g/T}$. Thus we note that if qps located near the BZ axis become gapped or lose their spectral weight at the Fermi level, the B_{1g} Raman slope and c -axis conductivity will show activated behavior while the B_{2g} Raman slope and the in-plane conductivity would continue to show metallic behavior. This is qualitatively the situation found for doping levels below $p_c \sim 0.22$ in all the cuprates. We note that the Raman measurements are not yet of sufficient precision to determine E_g from a fit since a straight line fit works well as shown in Fig. 2. More accurate data would be useful.

III. SUPERCONDUCTING STATE

We now consider how anisotropic transport in the normal state may be reflected in the superconducting state. In particular we would like to address whether the variant of the SS relation presented in Eq. (15) holds in the superconducting state.

In the absence of vertex corrections, the expressions for the Raman response and the optical conductivity in the static limit are given in terms of the Nambu Green’s functions as:

$$\begin{pmatrix} \sigma'_{\alpha,\beta}(T) \\ \partial\chi''_{\gamma,\gamma}(T)/\partial\Omega \end{pmatrix} = 2 \sum_{\mathbf{k}} \begin{pmatrix} j_{\mathbf{k}}^{\alpha} j_{\mathbf{k}}^{\beta} \\ \gamma_{\mathbf{k}}^2 \end{pmatrix} \quad (18)$$

$$\times \int \frac{dx}{\pi} \frac{\partial f(x)}{\partial x} \{ G''_0(\mathbf{k}, x)^2 + G''_3(\mathbf{k}, x)^2 \pm G''_1(\mathbf{k}, x)^2 \} .$$

Here $\hat{G}(\mathbf{k}, \omega) = \frac{1}{\tilde{\omega}\hat{\tau}_0 - \tilde{\epsilon}(\mathbf{k})\hat{\tau}_3 - \tilde{\Delta}(\mathbf{k})\hat{\tau}_1} = G_0(\mathbf{k}, \omega)\hat{\tau}_0 + G_1(\mathbf{k}, \omega)\hat{\tau}_1 + G_3(\mathbf{k}, \omega)\hat{\tau}_3$ with the renormalized quantities determined from the Pauli components of the self energy as $\tilde{\omega} = \omega - \Sigma_0(\mathbf{k}, \tilde{\omega})$, $\tilde{\epsilon}(\mathbf{k}) = \epsilon(\mathbf{k}) + \Sigma_3(\mathbf{k}, \tilde{\omega})$, and $\tilde{\Delta}(\mathbf{k}) = \Delta(\mathbf{k}) + \Sigma_1(\mathbf{k}, \tilde{\omega})$.

It is well known that vertex corrections appreciably alter universal results and the Wiedemann-Franz law for d -wave superconductors^{37,44,45}. In addition, they are crucially important for describing the back-flow needed to restore gauge-invariance in the superconducting state and appreciably alter the fully-symmetric A_{1g} response over a wide range of frequencies⁴⁶. Note that there are no Ward identities for Raman scattering apart from the fully symmetric charge channel, and generally vertex corrections do not appreciably alter the symmetry considerations which follow for the conductivities and the B_{1g} and B_{2g} Raman response. I therefore limit attention to σ_{xx}, σ_{zz} and the B_{1g} and B_{2g} Raman response. The reader is referred to Refs.^{37,44,45,46} where these issues have been addressed at length.

The self energy is usually broken into an inelastic term, such as due to phonons or spin-fluctuations, and an elastic term due to scattering from impurities: $\hat{\Sigma} = \hat{\Sigma}^{\text{inelastic}} + \hat{\Sigma}^{\text{elastic}}$ ⁴⁷. Since the integrand in Eq. (18) is weighted out for small frequencies and since $\Sigma''_{1,3}(\mathbf{k}, \tilde{\omega})$ coming from inelastic scattering are odd functions of frequency while $\Sigma''_0(\mathbf{k}, \tilde{\omega})$ is even, we only retain Σ_0 . If one considers s -wave impurity scattering in the Born or unitary limit, then $\Sigma_{1,3}^{\text{elastic}}$ can be neglected as well. However generally in other limits and in particular if the impurity potential is anisotropic as it should be in correlated systems, one must keep these terms as well^{37,44,47}.

In the next subsection the role of disorder in determining the asymptotic low temperature limit of the results functions is considered, and then in the following subsection, inelastic scattering from spin fluctuations is used to determine the full temperature dependence below T_c .

A. Disorder

We first consider scattering from point-like impurities to determine the low temperature limit of the response functions in the superconducting state. For s -wave impurity scattering $\tilde{\omega} = \omega - \Gamma \frac{\bar{g}_0}{c^2 - \bar{g}_0^2}$, with $\bar{g}_0 = \frac{1}{i} \langle \frac{\tilde{\omega}}{\tilde{\omega}^2 - \Delta^2(\mathbf{k})} \rangle$, $\Gamma = \frac{n_i}{\pi N_F}$, n_i the density of impurities, and c the phase shift²⁵. The self energy is determined self-consistently for temperatures below $T^* \sim n_i$ due to the formation of a bound-state impurity band at the Fermi level. In this limit, the solution may be expanded for small frequencies as $\tilde{\omega} = a\omega + i\gamma_0 + ib\omega^2$, with a, b and γ_0 determined from the impurity concentration and magnitude of the phase shift²⁶. Performing the standard integrals in Eq. (18) yields in the limit of low temperatures $T \ll T^*$

$$\begin{pmatrix} \sigma'_{\alpha,\beta}(T \ll T^*) \\ \partial\chi''_{\gamma,\gamma}(T \ll T^*)/\partial\Omega \end{pmatrix} = -N_F \int dx \frac{\partial f(x)}{\partial x}$$

$$\begin{aligned} & \times \left\{ \gamma_0^2 I_{3/2,0}^{\chi_{\gamma,\gamma},\sigma_{\alpha,\beta}} + x^2 \left[2b\gamma_0 I_{3/2,0}^{\chi_{\gamma,\gamma},\sigma_{\alpha,\beta}} + I_{5/2,0}^{\chi_{\gamma,\gamma},\sigma_{\alpha,\beta}} \right. \right. \\ & \times \left(\frac{15}{2}a^2\gamma_0^2 - 3b\gamma_0^2 \right) - \frac{15}{2}a^2\gamma_0^4 I_{7/2,0}^{\chi,\sigma} \\ & \left. \left. - \frac{5}{2}a^2\gamma_0^2 c^{\chi,\sigma} I_{7/2,1}^{\chi_{\gamma,\gamma},\sigma_{\alpha,\beta}} \right] \right\}, \end{aligned} \quad (19)$$

with the functions

$$\begin{aligned} I_{\nu,\mu}^{\chi_{\gamma,\gamma}} &= \left\langle \frac{\gamma^2(\mathbf{k})\Delta^\mu(\mathbf{k})}{[\gamma^2 + \Delta^2(\mathbf{k})]^\nu} \right\rangle, \\ I_{\nu,\mu}^{\sigma_{\alpha,\beta}} &= \left\langle \frac{v_\alpha(\mathbf{k})v_\beta(\mathbf{k})\Delta^\mu(\mathbf{k})}{[\gamma^2 + \Delta^2(\mathbf{k})]^\nu} \right\rangle, \end{aligned} \quad (20)$$

and the constant $c^{\chi,\sigma} = 2, 0$ for the Raman response and conductivity, respectively due to the different coherence factors. Eqs. (19 - 20) reduce to those found in Ref.⁴⁸ for the case of the $a - b$ plane conductivity. The functions $I_{\nu,\mu}^{\chi,\sigma}$ are straightforward to compute for a cylindrical FS and $\Delta(\mathbf{k}) = \Delta_0 \cos(2\phi)$. For resonant impurity scattering ($c = 0$), $a = 1/2$, $b = -\frac{1}{8\gamma_0}$, and γ_0 is determined self-consistently via $\gamma_0 = \sqrt{\frac{\pi\Gamma\Delta_0}{2\ln(4\Delta_0/\gamma_0)}}$ ²⁶. Eqs. (19-20) then yield:

$$\sigma'_{xx}(T \ll T^*) = \frac{ne^2}{m\pi\Delta_0} \left[1 + \frac{\pi^2}{12} \frac{T^2}{\gamma_0^2} \right], \quad (21)$$

$$\sigma'_{zz}(T \ll T^*) = \frac{ne^2}{m\pi\Delta_0} 2 \frac{v_z^2}{v_F^2} \frac{\gamma_0^2}{\Delta_0^2} \left[1 - \frac{\pi^2}{12} \frac{T^2}{\gamma_0^2} \right], \quad (22)$$

$$\frac{\partial \chi''_{B_{2g}}}{\partial \Omega}(T \ll T^*) = \frac{2N_F}{\pi\Delta_0} b_2^2 \left[1 + \frac{\pi^2}{36} \frac{T^2}{\gamma_0^2} \right], \quad (23)$$

$$\begin{aligned} \frac{\partial \chi''_{B_{1g}}}{\partial \Omega}(T \ll T^*) &= \frac{2N_F}{\pi\Delta_0} b_1^2 \frac{\gamma_0^2}{\Delta_0^2} \ln(4\Delta_0/\gamma_0) \\ &\times \left[1 - \frac{\pi^2}{12} \frac{T^2}{\gamma_0^2} \right], \end{aligned} \quad (24)$$

where n is the 2D electron density. Eq. (21) for the in-plane conductivity has been derived several times^{26,37,48,49}, and Eqs. (23-24) for the Raman slope are identical to those found in Ref.³². The result for the out-of-plane conductivity for $T = 0$ is also in agreement with the result from Ref.⁹, but the temperature dependent variation has not been presented before. We note as in Refs.^{26,31,32,37,48,49} that both the in-plane conductivity and the B_{2g} Raman slope are universal numbers for resonant scattering independent of the strength of the scattering, while both the c -axis conductivity and the B_{1g} Raman slope depend on γ_0 . The γ_0 dependence does not appear in the c -axis conductivity if the c -axis hopping is taken as a constant independent of direction around the FS^{9,50}. The temperature dependencies are *positive* for both the in-plane conductivity and the B_{2g} slope, but are *negative* for the out-of-plane conductivity and the B_{1g} slope, giving a peak at zero T for the latter pair. We note that this result is in agreement with the rise of the c -axis conductivity recently observed in $\text{YBa}_2\text{Cu}_3\text{O}_{6.95}$ at low temperatures³⁰.

In the limit of higher temperatures $T_c \gg T \gg T^*$ where the density of states does not have an impurity induced weight at the Fermi level and matches the DOS from the clean limit, the self consistency is not required for the self energy and Eq. (18) can be rewritten as

$$\begin{aligned} & \left(\begin{array}{l} \sigma'_{\alpha,\beta}(T^* \ll T \ll T_c) \\ \partial \chi''_{\gamma,\gamma}(T^* \ll T \ll T_c) / \partial \Omega \end{array} \right) = \\ & -2N_F \int dx \frac{\partial f(x)}{\partial x} \text{Im} \left[\frac{1}{\Omega - i/\tau(x)} \right] \\ & \times \left\langle \left(\begin{array}{l} v_\alpha(\mathbf{k})v_\beta(\mathbf{k}) \\ \gamma^2(\mathbf{k}) \end{array} \right) \text{Re} \left[\frac{x}{\sqrt{x^2 - \Delta(\mathbf{k})^2}} \right] \right\rangle, \end{aligned} \quad (25)$$

with $1/\tau(x) = -2\Sigma''_0(x)$. This is a generalization of the results obtained in Refs.^{11,12,26} to the case of Raman and optical conductivity. We note that for d -wave superconductors in the resonant limit, the impurity scattering rate depends strongly on frequency

$$1/\tau(\omega \rightarrow 0) = \frac{\pi^2\Gamma\Delta_0}{2\omega} \frac{1}{\ln^2(4\Delta_0/\omega)}, \quad (26)$$

as shown in Ref.²⁶, which yields

$$\begin{aligned} & \left(\begin{array}{l} \sigma'_{\alpha,\beta}(T^* \ll T \ll T_c) \\ \partial \chi''_{\gamma,\gamma}(T^* \ll T \ll T_c) / \partial \Omega \end{array} \right) = \\ & -\frac{4N_F}{\pi^2} \frac{T^2}{\Gamma\Delta_0} \int dz z^2 \frac{e^z}{(e^z + 1)^2} \\ & \times \ln^2(4\Delta_0/zT) H^{\sigma_{\alpha,\beta},\chi_{\gamma,\gamma}}(zT), \end{aligned} \quad (27)$$

with the functions

$$H^{\sigma_{\alpha,\beta}}(x) = \text{Re} \left\langle \frac{v_\alpha(\mathbf{k})v_\beta(\mathbf{k})}{\sqrt{x^2 - \Delta(\mathbf{k})^2}} \right\rangle, \quad (28)$$

$$H^{\chi_{\gamma,\gamma}}(x) = \text{Re} \left\langle \frac{\gamma^2(\mathbf{k})}{\sqrt{x^2 - \Delta(\mathbf{k})^2}} \right\rangle. \quad (29)$$

Performing the integrals gives for small x gives

$$H^{\chi_{\gamma,\gamma}}(x) = \begin{cases} \frac{x^2}{2\Delta_0^3}, & B_{1g}, \\ \frac{1}{\Delta_0}, & B_{2g}, \end{cases} \quad (30)$$

$$H^{\sigma_{\alpha,\beta}}(x) = \begin{cases} \frac{1}{2\Delta_0}, & \sigma_{xx}, \\ \frac{x^2}{4\Delta_0^3}, & \sigma_{zz}. \end{cases} \quad (31)$$

The remaining integrals in Eq. (27) can be easily performed:

$$\begin{aligned} & \sigma'_{\alpha,\beta}(T^* \ll T \ll T_c) = \\ & \begin{cases} \frac{2ne^2}{3m\Gamma} \frac{\Delta_0^2}{T^2} \ln^2\left(\frac{4\Delta_0}{T}\right), & \sigma_{xx}, \\ \frac{14\pi^2 ne^2 v_z^2}{15m\Gamma v_F^2} \left(\frac{T}{\Delta_0}\right)^4 \ln^2\left(\frac{4\Delta_0}{T}\right), & \sigma_{zz}, \end{cases} \end{aligned} \quad (32)$$

$$\begin{aligned} & \frac{\partial \chi''_{\gamma,\gamma}(T^* \ll T \ll T_c)}{\partial \Omega} = \\ & \begin{cases} \frac{4b_2^2 N_F}{3\Gamma} \left(\frac{T}{\Delta_0}\right)^2 \ln^2\left(\frac{4\Delta_0}{T}\right), & B_{2g}, \\ \frac{14\pi^2 b_1^2 N_F}{15\Gamma} \left(\frac{T}{\Delta_0}\right)^4 \ln^2\left(\frac{4\Delta_0}{T}\right), & B_{1g}. \end{cases} \end{aligned} \quad (33)$$

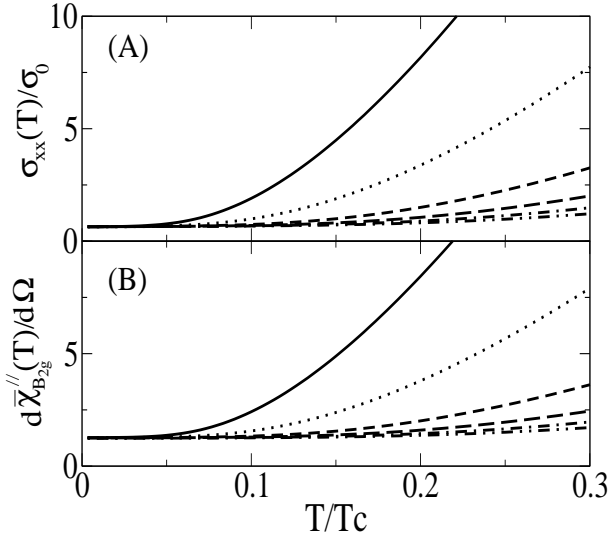


FIG. 4: Temperature dependence of the in-plane conductivity (Panel A) and the B_{2g} Raman slope (Panel B) for resonant scattering and different impurity scattering strengths $\Gamma/\Delta_0 = 0.004, 0.008, 0.016, 0.024$ and 0.04 (solid, dotted, short-dashed, long-dashed, and dotted-dashed lines), respectively, for $\Delta_0/T_c = 4$. Here $\sigma_0 = N_F e^2 v_F^2$ and $\bar{\chi}'' = \chi''/N_F b_2^2$ are the dimensionless quantities shown.

The expression for the in-plane conductivity was derived in Ref.²⁶ but to our knowledge the other terms are new. We note the results for σ_{zz} and σ_{xx} in this limit differ from those obtain in Ref.¹², where a frequency independent scattering time was used rather than that of Eq. (26). As a consequence they concluded that $\sigma_{xx,zz}(T) \propto n_{xx,zz}(T)$ with $n_{xx,zz}(T)$ the normal-fluid density which decreases uniformly with temperature in contrast to experiments³⁰. From that they concluded that the scattering time must be anisotropic. We note that any frequency dependence of the scattering time would qualitatively change this conclusion.

The results of Eqs. (21-24) and (32-33) imply that the SS relations in the normal state Eq. (15) hold in the superconducting state. The exponent of the low temperature rise *as well as the sign of the correction* do obey the general scaling relation, following simply from the interplay of anisotropies of $\Delta(\mathbf{k})$ and the respective vertices.

The response for $T \ll T_c$ is calculated by numerically solving Eq. 18 and the corresponding self-consistent equations to determine the self energies. The results for $\sigma_{xx}(T), \partial\chi''_{B_{2g}}(T)/\partial\Omega$, and $\sigma_{zz}(T), \partial\chi''_{B_{1g}}(T)/\partial\Omega$ are shown in Figures 4 and 5, respectively, for resonant scattering and different values of the impurity scattering strengths Γ/Δ_0 . Generally at higher temperatures $T > T^*$ all quantities increase rapidly with temperature, rising as T^2 and T^4 for $\sigma_{xx}, \partial\chi_{B_{2g}}/\partial\Omega$ and $\sigma_{zz}, \partial\chi_{B_{1g}}/\partial\Omega$, respectively. The rise of the c -axis conductivity and the B_{1g} Raman slope at low temperatures shown in the insets of Fig. 5 are generally on the order of a few percent for the parameters shown. This height rises for smaller

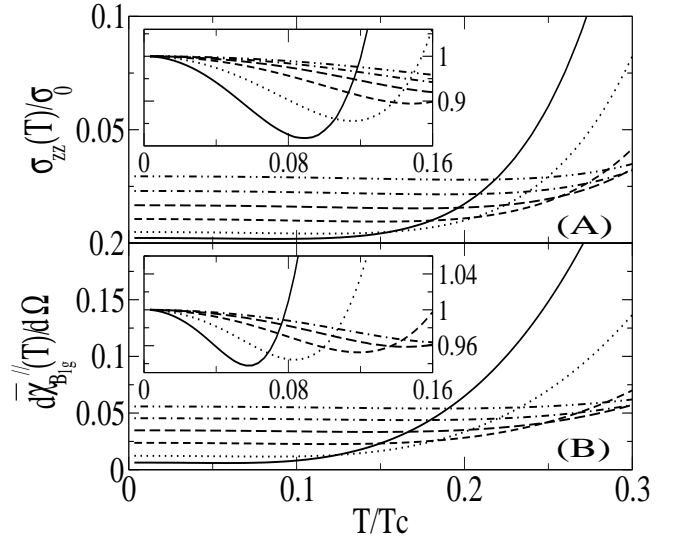


FIG. 5: Temperature dependence of the out-of-plane conductivity (Panel A) and the B_{1g} Raman slope (Panel B) for resonant scattering ($c=0$) and different impurity scattering strengths $\Gamma/\Delta_0 = 0.004, 0.008, 0.016, 0.024$ and 0.04 (solid, dotted, short-dashed, long-dashed, and dotted-dashed lines), respectively, for $\Delta_0/T_c = 4$. Here $\sigma_0 = N_F e^2 v_z^2$ and $\bar{\chi}'' = \chi''/N_F b_1^2$ are the dimensionless quantities shown. The insets show the low temperature rise of both σ_{zz} and $\partial\chi''/\partial\Omega$ (normalized to their zero temperature values) with decreasing temperature.

values of Γ but onsets at smaller temperatures due to the concomitant reduction in T^* . In particular, the rise and the onset of the c -axis conductivity low temperature maximum for $\text{YBa}_2\text{Cu}_3\text{O}_{6.95}$ ³⁰ cannot be adequately reproduced. There are as yet no Raman measurements to compare to, and thus it would be extremely useful to have data on a wide range of compounds and doping levels as well as a systematic check of impurity doping effects to test these results.

B. Spin fluctuations

The different rate of descent of the response functions below T_c has an interesting consequence on the conductivity peak seen in *ab*-plane measurements and the lack of peak seen in c -axis measurements. Ref.²⁶ included inelastic scattering from spin fluctuations in RPA to reproduce the *ab*-peak in the conductivity observed in Ref.^{23,24}. In Refs.^{12,26} it was shown that Eq. (25) for the conductivities for $T_c \gg T \gg T^*$ may be reexpressed in terms of the normal qp density which can be generalized as

$$\sigma_{\alpha,\beta}(T) = \frac{n_{qp}^{\alpha\beta}(T)e^2}{m}\bar{\tau}, \quad (34)$$

with

$$n_{qp}^{\alpha,\beta}(T) = \frac{1}{v_F^2} \int d\omega \left\langle \text{Re} \left[\frac{v_\alpha(\mathbf{k})v_\beta(\mathbf{k})\omega}{\sqrt{\omega^2 - \Delta(\mathbf{k})^2}} \right] \right\rangle \left[-\frac{\partial f}{\partial \omega} \right] \quad (35)$$

the projected normal quasiparticle density. The average $\bar{\tau}$ is derived from the frequency-dependent $\tau(\omega)$ and the superconducting density of states $N(\omega)$ as

$$\bar{\tau} = \frac{\int d\omega N(\omega)(-\partial f/\partial \omega)\tau(\omega)}{\int d\omega N(\omega)(-\partial f/\partial \omega)}. \quad (36)$$

Similarly one can re-express the Raman slopes in the same fashion:

$$\partial\chi''_{\gamma,\gamma}(T)/\partial\Omega = n_{qp}^{R,\gamma\gamma}(T)\bar{\tau}, \quad (37)$$

with

$$n_{qp}^{R,\gamma\gamma}(T) = \int d\omega \left\langle \text{Re} \left[\frac{\gamma^2(\mathbf{k})\omega}{\sqrt{\omega^2 - \Delta(\mathbf{k})^2}} \right] \right\rangle \left[-\frac{\partial f}{\partial \omega} \right] \quad (38)$$

the Raman projected normal qp density. For a $d_{x^2-y^2}$ gap, from the results of Eqs. (28-31) the projected qp densities at low T vary as T for $n_{qp}^{xx}, n_{qp}^{R,B_{2g}}$ and T^3 for $n_{qp}^{zz}, n_{qp}^{R,B_{1g}}$, respectively. If the scattering time τ were independent of frequency, then n_{qp} gives the full temperature dependence and thus $\sigma_{xx}, \partial\chi''_{B_{2g}}/\partial\Omega$ would vary linearly with T and $\sigma_{zz}, \partial\chi''_{B_{1g}}/\partial\Omega$ would vary as T^3 . Ref.¹² used this result for σ_{zz} and argued that T^3 accurately fit the data for $T > 40K$, but they could not explain the rise at low T . However, the impurity scattering rate as well as the scattering due to inelastic collisions, such as spin fluctuations, depend on momentum and strongly depend on both temperature and frequency. The latter is crucially needed in order to explain the peak in the *ab*-plane conductivity.

Refs.^{25,26,44} utilized calculations of the inelastic scattering due to spin fluctuations in the 2D Hubbard model in the Random Phase approximation (RPA) for $U = 2t$ to describe the dc and IR conductivity and the frequency dependent Raman response. The lifetime calculated for $U = 2t$ and $\Delta_0/T_c = 3 - 4$ ⁵¹ was found to give reasonable agreement with the transport lifetime determined from conductivity measurements in Y-123²⁴ and gave reasonable agreement with the *ab*-plane conductivity peak²⁶, *ab*-plane IR conductivity response²⁵, and simultaneously the *ab*-plane IR and the B_{1g} and B_{2g} Raman response in Bi-2212⁴⁴. We therefore use this approach to calculate the temperature dependence of the response functions for all temperatures below T_c .

In RPA, the self energy Σ_0 is given from the effective potential V as:

$$V(\mathbf{q}, i\Omega) = \frac{3}{2} \frac{\bar{U}^2 \chi_0(\mathbf{q}, i\Omega)}{1 - \bar{U} \chi_0(\mathbf{q}, i\Omega)}, \quad (39)$$

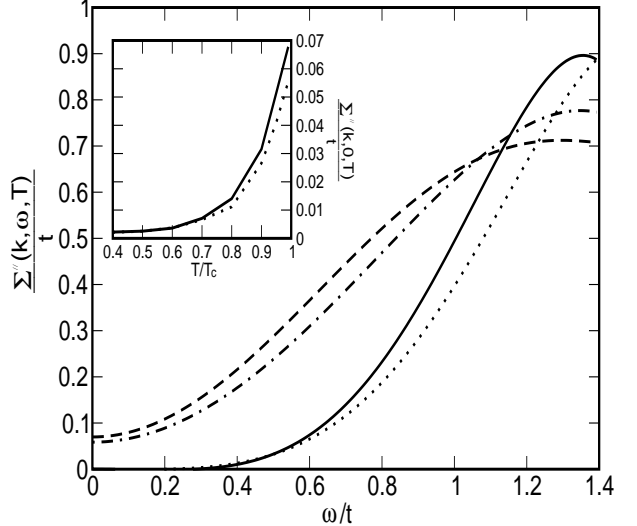


FIG. 6: Frequency dependence of the imaginary part of the $\hat{\tau}_0$ self energy $\Sigma_0''(\mathbf{k}, \omega, T)$ normalized to the hopping overlap t as a function of frequency and temperature for different points in the BZ. The solid line and dotted line are for $T = 0.5T_c$ for gap maximum $\mathbf{k} = (\pi/a, 0)$ and gap node $(\pi/2a, \pi/2a)$ point, respectively, while the dashed and dot-dashed lines correspond to the gap max and gap node points at T_c . The inset shows the zero frequency part of Σ_0'' as a function of temperature.

where \bar{U} is a phenomenological parameter [we choose $\bar{U} = 2t$]. $\chi_0(\mathbf{q}, i\Omega)$ is the non-interacting spin susceptibility,

$$\chi_0(\mathbf{q}, i\Omega) = \sum_{\mathbf{k}} \left\{ \frac{a_{\mathbf{k},\mathbf{k}+\mathbf{q}}^+}{2N} \frac{f(E_{\mathbf{k}+\mathbf{q}}) - f(E_{\mathbf{k}})}{i\Omega - (E_{\mathbf{k}+\mathbf{q}} - E_{\mathbf{k}})} + \frac{a_{\mathbf{k},\mathbf{k}+\mathbf{q}}^-}{4N} \left[\frac{1 - f(E_{\mathbf{k}+\mathbf{q}}) - f(E_{\mathbf{k}})}{i\Omega + E_{\mathbf{k}+\mathbf{q}} + E_{\mathbf{k}}} - \frac{1 - f(E_{\mathbf{k}+\mathbf{q}}) - f(E_{\mathbf{k}})}{i\Omega - E_{\mathbf{k}+\mathbf{q}} - E_{\mathbf{k}}} \right] \right\}. \quad (40)$$

Here $E_{\mathbf{k}}^2 = \epsilon_{\mathbf{k}}^2 + \Delta_{\mathbf{k}}^2$ and the coherence factors are $a_{\mathbf{k},\mathbf{k}+\mathbf{q}}^{\pm} = 1 \pm \frac{\epsilon_{\mathbf{k}+\mathbf{q}}\epsilon_{\mathbf{k}} + \Delta_{\mathbf{k}}\Delta_{\mathbf{k}+\mathbf{q}}}{E_{\mathbf{k}+\mathbf{q}}E_{\mathbf{k}}}$. This yields a self energy

$$\hat{\Sigma}(\mathbf{k}, i\omega) = - \int \frac{dx}{\pi N} \sum_{\mathbf{q}} V''(\mathbf{q}, x) \frac{1}{2E_{\mathbf{k}-\mathbf{q}}} \left[\frac{E_{\mathbf{k}-\mathbf{q}}\hat{\tau}_0 + \epsilon_{\mathbf{k}-\mathbf{q}}\hat{\tau}_3 + \Delta_{\mathbf{k}-\mathbf{q}}\hat{\tau}_1}{E_{\mathbf{k}-\mathbf{q}} + x - i\omega} [n(x) + f(-E_{\mathbf{k}-\mathbf{q}})] - \frac{-E_{\mathbf{k}-\mathbf{q}}\hat{\tau}_0 + \epsilon_{\mathbf{k}-\mathbf{q}}\hat{\tau}_3 + \Delta_{\mathbf{k}-\mathbf{q}}\hat{\tau}_1}{-E_{\mathbf{k}-\mathbf{q}} + x - i\omega} [n(x) + f(E_{\mathbf{k}-\mathbf{q}})] \right] \quad (41)$$

with n the Bose factor.

The imaginary part of the $\hat{\tau}_0$ self energy $\Sigma_0''(\mathbf{k}, \omega, T)$ normalized to the hopping overlap t as a function of frequency and temperature for different points in the BZ is shown in Fig. (6). Here we have used the band structure $\epsilon_{\mathbf{k}}$ as in (A4) in the appendix with $t'/t = 0.45$ and a filling $n = 0.88$, $U = 2t$, and a $d_{x^2-y^2}$ energy gap $\Delta_{\mathbf{k}} = \Delta_0[\cos(k_x a) - \cos(k_y a)]/2$ with $\Delta_0/t = 0.4 = 4T_c$. The solid line and dotted line shows the frequency dependence of Σ'' at a temperature $T = 0.5T_c$ for gap maximum $\mathbf{k} = (\pi/a, 0)$ and gap node $(\pi/2a, \pi/2a)$, respectively, while the dashed and dot-dashed lines correspond

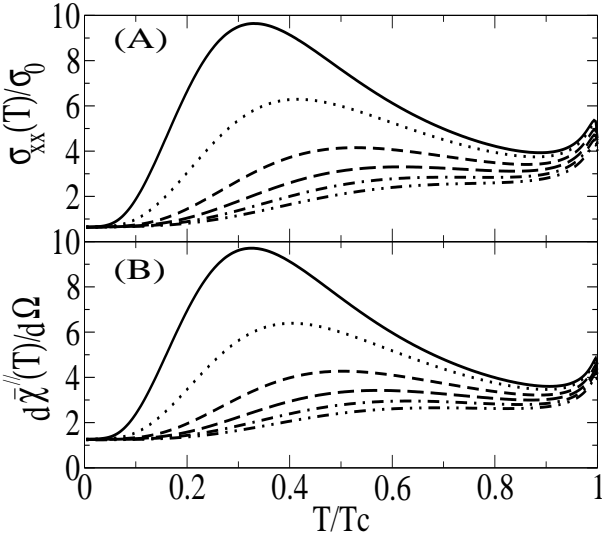


FIG. 7: Temperature dependence of the in-plane conductivity (Panel A) and the B_{2g} Raman slope (Panel B) including inelastic spin fluctuations and resonant impurity scattering for different impurity scattering strengths $\Gamma/\Delta_0 = 0.004, 0.008, 0.016, 0.024$ and 0.04 (solid, dotted, short-dashed, long-dashed, and dotted-dashed lines), respectively, for $\Delta_0/T_c = 4$. Here $\sigma_0 = N_F e^2 v_F^2$ and $\bar{\chi}'' = \chi''/N_F b_2^2$ are the dimensionless quantities shown.

to the gap max and gap node points at T_c . The differences for the gap maximum and gap node points are not too strong and can be adequately fit with a threshold behavior $\sim (\omega - 3\Delta(\mathbf{k}))^3$ plus a temperature dependent part which also depends on momentum. The inset shows the zero frequency part of Σ_0'' as a function of temperature. Except for low temperatures where the nodal properties of the interaction govern the behavior, the momentum dependence of the self energy is weak and can be adequately modelled by a temperature dependent $\sim T^3$ term plus a frequency dependent part $\sim \omega^3$.

In an effort to address the temperature dependence of these quantities, we employ a simple parameterized fit to the numerical results for $1/\tau_{\mathbf{k}}(\omega, T) = -2\Sigma_0''(\mathbf{k}, \omega, T)$ determined from Eq. (41) and Fig. (8) and add that to the elastic contribution calculated in the last section. Assuming Matthiessen's law to hold in this case neglects vertex corrections and the joint influence of disorder on the spin fluctuations and vice-versa, but for weak disorder should be sufficient to capture the qualitative behavior of various quantities derived on the FS.

The results for the four response functions derived from Eq. (18) are shown in Figures 7 and 8. Both the in-plane conductivity (Fig. 7A) and the B_{2g} Raman slope (Fig. 7B) possess a peak near $T \sim 0.3T_c$ for $\Gamma/\Delta_0 = 0.004$ which decreases in height and moves to higher temperatures for increasing impurity scattering. It is important to emphasize that this peak is not related to coherence effects and is a simple balance of fall-off of the inelastic scattering rate $\sim T^3$ and the rise of the impurity scattering rate $\sim 1/T$ at low temperatures. The sum of these

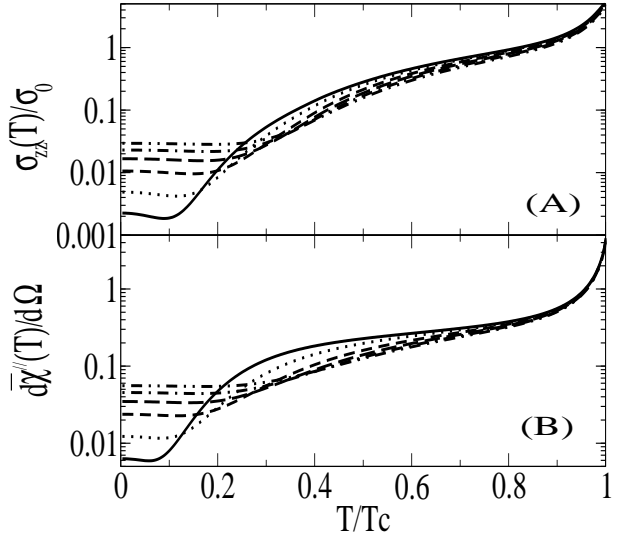


FIG. 8: Temperature dependence of the out-of-plane conductivity σ_{zz} (Panel A) and the B_{1g} Raman slope (Panel B) including inelastic spin fluctuations and resonant impurity scattering for different impurity scattering strengths $\Gamma/\Delta_0 = 0.004, 0.008, 0.016, 0.024$ and 0.04 (solid, dotted, short-dashed, long-dashed, and dotted-dashed lines), respectively, for $\Delta_0/T_c = 4$. Here $\sigma_0 = N_F e^2 v_F^2$ and $\bar{\chi}'' = \chi''/N_F b_1^2$ are the dimensionless quantities shown.

scattering rates is multiplied by the normal qp density $\propto T$ at low temperatures, as shown in Eqs. (27) and (33), and therefore σ_{xx} and $\partial\chi''_{B_{2g}}/\partial\Omega$ vary as $1/T^2$ for $T^* < T < T_c$ and approach a universal constant in the zero temperature limit.

However, no corresponding peak is found for both the out-of-plane conductivity (Fig. 8A) and B_{1g} Raman slope (Fig. 8B), in agreement with experimental observations. The curves simply show a rapid fall off of both quantities for $T < T_c$ and a small rise of both quantities which onsets at T^* and reaches a zero temperature maximum as shown in Fig. 5. The main difference is due to the behavior of zone-axis projected qp density, which varies as T^3 at low temperatures, with a factor of T coming from the nodes and the additional T^2 coming from the matrix elements. This compensates the $1/T^3$ rise of the qp inelastic lifetime, and both σ_{zz} and $\partial\chi''_{B_{1g}}/\partial\Omega$ vary as T^μ for $T \gg T^*$ with μ dependent on the strength of the impurity scattering, and rise for $T \ll T^*$, as shown in Fig. (5). For example, for the parameters chosen in Fig. (8), the exponent μ for $0.3T_c < T < 0.9T_c$ for the c -axis conductivity $\sigma_{zz}(T)$ varies from 2.7 to 3.4 for increasing impurity scattering. If the frequency dependence of the scattering rate were neglected, then a universal exponent $\mu = 3$ would emerge¹². Therefore it would be highly useful if further systematic checks were performed and Raman data were available to compare to the conductivity and the theoretical predictions.

IV. SUMMARY AND CONCLUSIONS

In summary, based on symmetry arguments we have demonstrated how the relaxational behavior of the qp in the cuprates should manifest itself in the various experiments and how the results are expected to be interrelated. Therefore, a single framework may relate the optically-derived qp scattering rates to transport measurements to infer charge dynamics on different regions of the Brillouin zone. Using forms for the interlayer hopping and qp self energy consistent with empirical evidence, a variant of the SS relation was shown to relate the zone-diagonal and zone-axis transport properties measured by DC conductivity and the slope of the Raman response in the normal state, in agreement with experimental observations in Bi-2212 and Y-123, but not La-214. The “scattering ratios” show power-law behavior for the Raman response which can be reasonably accounted for in several models near optimal doping. However no single model can adequately describe the data over the entire doping range, indicating that additional physics related to quantum critical behavior is required²².

In the superconducting state, a similar SS relation is found which arises from the momentum dependence of the energy gap and conductivity and Raman matrix elements. In particular, we found that the a zero temperature peak is predicted to arise in σ_{zz} and $\partial\chi''_{B_{1g}}/\partial\Omega$ without the presence of a maximum near $0.3T_c$ found for σ_{xx} and $\partial\chi''_{B_{1g}}/\partial\Omega$. The results are in rough, qualitative agreement with the available data for σ_{zz} but the strength of the elastic scattering cannot simultaneously account for in-plane and out-of-plane conductivities. However, the simple model presented does not account for anisotropies in impurity scattering, known to arise for point-like scatterers in correlated materials. It would be useful to test if the data can be explained by invoking anisotropic impurity potentials. Unfortunately, Raman data in the superconducting state to further test the theory is lacking. In particular, it would be extremely useful to determine if the deviations from the derived SS relation observed in the normal state of La-214 carry over into the superconducting state.

The agreement of the derived SS relations in both the superconducting and normal states with the available data on Bi-2212 and Y-123 indicate that the in-plane momentum is at least partially conserved in c-axis transport over the entire doping range studied. This shows that in principle a comparison of Raman and transport could eventually contribute to the solution of the c-axis transport problem. Deviations which result in a finite c-axis hopping along the BZ diagonals would invalidate the derived scaling relations, but if the hopping is small along the diagonals then a violation could only be seen at very low temperatures. Finally, we point out that a quantitative study of the interrelation of the various response functions require the inclusion of vertex corrections in order to explore the influence of the relevant interactions between the electrons. This however reaches beyond the

scope of the present work.

Acknowledgments

The author would like to thank R. Hackl and F. Venturini for numerous discussions, and gratefully acknowledges support from NSERC and from PREA.

APPENDIX A

We start by considering a four band model for the CuO_2 plane with $Cu_{3d} - O_{p_{x,y}}$ hopping amplitude t_{pd} , $Cu_{4s} - O_{p_{x,y}}$ hopping amplitude t_{ps} , $O_{p_x} - O_{p_y}$ hopping amplitude t_{pp} , and c-axis Cu_{4s} - Cu_{4s} amplitude t_s , respectively:

$$\begin{aligned}
 H = & \epsilon_d \sum_{\mathbf{n},\sigma} d_{\mathbf{n},\sigma}^\dagger d_{\mathbf{n},\sigma} + \epsilon_s \sum_{\mathbf{n},\sigma} s_{\mathbf{n},\sigma}^\dagger s_{\mathbf{n},\sigma} \\
 & - t_{pd} \sum_{\mathbf{n},\delta,\sigma} P_\delta (d_{\mathbf{n},\sigma}^\dagger a_{\mathbf{n},\delta,\sigma} + h.c.) \\
 & - t_{pp} \sum_{\mathbf{n},\delta,\delta',\sigma} P'_{\delta,\delta'} a_{\mathbf{n},\delta,\sigma}^\dagger a_{\mathbf{n},\delta',\sigma} \\
 & - t_{ps} \sum_{\mathbf{n},\delta,\sigma} P''_\delta (s_{\mathbf{n},\sigma}^\dagger a_{\mathbf{n},\delta,\sigma} + h.c.) \\
 & - t_s \sum_{\langle \mathbf{n},\mathbf{m} \rangle, \sigma} s_{\mathbf{n},\sigma}^\dagger s_{\mathbf{m},\sigma}, \tag{A1}
 \end{aligned}$$

where $\epsilon_{s,d} = E_{s,d} - E_p$ represents the charge transfer energy from the oxygen p - to $Cu_{4s,3d}$ orbitals, respectively. Here $s_{\mathbf{n},\sigma}^\dagger, d_{\mathbf{n},\sigma}^\dagger$ creates an $4s, 3d_{x^2-y^2}$ electron, respectively, with spin σ at a copper lattice site \mathbf{n} , while $a_{\mathbf{n},\delta,\sigma}$ annihilates an electron at one of the neighboring oxygen sites $\mathbf{n} + \delta/2$ determined by the unit vector δ assuming the four values, $(\pm 1, 0)$ and $(0, \pm 1)$. The overlap factors P have the following properties: $P_{(1,0)} = P''_{(1,0)} = 1, P_{(0,1)} = P''_{(0,1)} = -1, P'_{\mathbf{x},\mathbf{y}} = P'_{-\mathbf{x},-\mathbf{y}} = 1, P'_{-\mathbf{x},\mathbf{y}} = P'_{\mathbf{x},-\mathbf{y}} = -1$, respectively. Lastly the bracket $\langle \dots \rangle$ notes a sum over the nearest neighbor Cu_{4s} sites in the c -direction. Thus c -axis hopping is mediated by the Cu_{4s} orbitals hybridizing with the bonding and anti-bonding pd bands consistent with LDA²⁰.

After Fourier transforming, the Hamiltonian is $H = \sum_{\mathbf{k},\sigma} H_{\mathbf{k},\sigma}$ with

$$\begin{aligned}
 H_{\mathbf{k},\sigma} = & \epsilon_d d_{\mathbf{k},\sigma}^\dagger d_{\mathbf{k},\sigma} + \epsilon_s(\mathbf{k}) s_{\mathbf{k},\sigma}^\dagger s_{\mathbf{k},\sigma} \\
 & - \{2it_{pd} d_{\mathbf{k},\sigma}^\dagger [a_{x,\mathbf{k},\sigma} s_x(\mathbf{k}) - a_{y,\mathbf{k},\sigma} s_y(\mathbf{k})] + h.c.\} \\
 & - \{2it_{ps} s_{\mathbf{k},\sigma}^\dagger [a_{x,\mathbf{k},\sigma} s_x(\mathbf{k}) + a_{y,\mathbf{k},\sigma} s_y(\mathbf{k})] + h.c.\} \\
 & - 4t_{pp} s_x(\mathbf{k}) s_y(\mathbf{k}) [a_{x,\mathbf{k},\sigma}^\dagger a_{y,\mathbf{k},\sigma} + h.c.], \tag{A2}
 \end{aligned}$$

with $s_\alpha(\mathbf{k}) = \sin(ak_\alpha/2)$ and $\epsilon_s(\mathbf{k}) = \epsilon_s - 2t_{ss} \cos(k_z c)$. Eq. A2 can be diagonalized by defining “canonical

fermions”⁵³:

$$\begin{aligned}\alpha_{\mathbf{k},\sigma} &= i \frac{s_x(\mathbf{k})a_{x,\mathbf{k},\sigma} - s_y(\mathbf{k})a_{y,\mathbf{k},\sigma}}{\mu(\mathbf{k})} \\ \beta_{\mathbf{k},\sigma} &= -i \frac{s_y(\mathbf{k})a_{x,\mathbf{k},\sigma} + s_x(\mathbf{k})a_{y,\mathbf{k},\sigma}}{\mu(\mathbf{k})},\end{aligned}\quad (\text{A3})$$

where $\mu(\mathbf{k})^2 = s_x^2(\mathbf{k}) + s_y^2(\mathbf{k})$. This gives anti-bonding, bonding bands hybridized with the Cu orbitals. This four-band model can be reduced to an effective one-band model by eliminating the β band and the two bands with high energies $\sim \epsilon_{s,d}$. This is achieved by defining two other sets of canonical fermions and expanding in powers of $t_{pd,pd,ss}/\epsilon_{s,d}$ ⁵⁴. The single-band dispersion is approximately given by

$$\epsilon(\mathbf{k}) = -2t[\cos(k_x a) + \cos(k_y a)] + 4t' \cos(k_x a) \cos(k_y a)$$

$$\begin{aligned}&-2t'' \cos(2k_x a) \cos(2k_y a) \\ &-t_{\perp} \cos(k_z c)[\cos(k_x a) - \cos(k_y a)]^2 - \mu,\end{aligned}\quad (\text{A4})$$

with the identification to lowest order of $t = t_{pp} - t_{pd}^2/\epsilon_d$, $t' = -t_{pp}/2 + t_{ps}^2/8\epsilon_s$, $t'' = t_{ps}^2/16\epsilon_s$, and $t_{\perp} = t_{ss}t_{ps}^2/\epsilon_s^2$. This form for the interplane hopping can also be derived in the framework of the Hubbard model by projecting out the high-lying Cu 4s orbitals and the high-lying $d-p$ spin triplets by solving the correlation problem within the unit cell and treating the intercell hopping as a degeneracy lifting perturbation^{11,53}.

- ¹ S. L. Cooper and K. E. Gray, in *Physical Properties of High-Temperature Superconductors IV*, edited by D. M. Ginsberg (World Scientific, Singapore, 1994).
- ² S. V. Dordevic, E. J. Singley, D. N. Basov, S. Komiya, Y. Ando, E. Bucher, C. C. Homes and M. Strongin, Phys. Rev. B **65**, 134511 (2002); S. Tajima, J. Schützmann, S. Miyamoto, I. Terasaki, Y. Sato, and R. Hauff, Phys. Rev. B **55**, 6051 (1997).
- ³ T. Watanabe, T. Fujii, and A. Matsuda, Phys. Rev. Lett. **79**, 2113 (1997).
- ⁴ C. Kendziora, M. C. Martin, J. Haartge, L. Mihaly, and L. Forró, Phys. Rev. B **48**, 3531 (1993).
- ⁵ L. Forró, Phys. Lett. A **179**, 140 (1993).
- ⁶ D. N. Basov, S. I. Woods, A. S. Katz, E. J. Singley, R. C. Dynes, M. Xu, D. G. Hinks, C. C. Homes, and M. Strongin, Science **283**, 49 (1999); D. N. Basov, C. C. Homes, E. J. Singley, M. Strongin, T. Timusk, G. Blumberg, and D. van der Marel, Phys. Rev. B **63**, 134514 (2001); H. J. A. Molegraaf, C. Presura, D. van der Marel, P. H. Kes, and M. Li, Science **295**, 2239 (2002).
- ⁷ P. W. Anderson, *The Theory of Superconductivity in the High T_c Cuprates* (Princeton University Press, Princeton, 1997); A. J. Leggett, Phys. Rev. Lett. **83**, 392 (1999); M. Turlakov and A. J. Leggett, Phys. Rev. B **63**, 64518 (2001).
- ⁸ L. B. Ioffe and A. J. Millis, **285**, 1241 (1999); Phys. Rev. B **61**, 9077 (2000); N. Shah and A. J. Millis, Phys. Rev. B **64**, 174506 (2001); **65**, 024506 (2001).
- ⁹ W. Kim and J. P. Carbotte, Phys. Rev. B **63**, 054526 (2001); E. Schachinger and J. P. Carbotte, Phys. Rev. B **64**, 94501 (2001).
- ¹⁰ P. S. Cornaglia, K. Hallberg, and C. A. Balseiro, Phys. Rev. B **63**, 060504 (2001).
- ¹¹ T. Xiang and J. M. Wheatley, Phys. Rev. Lett. **77**, 4632 (1996).
- ¹² T. Xiang and W. Hardy, Phys. Rev. B **63**, 024506 (2000).
- ¹³ D. van der Marel, Phys. Rev. B **60**, 765 (1999).
- ¹⁴ L. B. Ioffe and A. J. Millis, Phys. Rev. B **58**, 11631 (1998).
- ¹⁵ R. Hlubina and T. M. Rice, Phys. Rev. B **51**, 9253 (1995); D. Pines and B. Stojković **55**, 8576 (1997); **56**, 11931 (1997); R. Hlubina, Phys. Rev. B **58**, 8240 (1998).
- ¹⁶ P. Coleman, A. J. Schofield, and A. M. Tsvelik, Phys. Rev. Lett. **76**, 1324 (1996); A. T. Zheleznyak, V. M. Yakovenko, H. D. Drew, and I. I. Mazin, Phys. Rev. B **57**, 3089 (1998); **59**, 207 (1999); K. G. Sandeman and A. J. Schofield, Phys. Rev. B **63**, 094510 (2001).
- ¹⁷ E. Abrahams and C. M. Varma, Phys. Rev. Lett. **86**, 4652 (2001); **88**, 139903 (2002).
- ¹⁸ A. A. Abrikosov, Physica C **258**, 53 (1996).
- ¹⁹ W. A. Atkinson and J. P. Carbotte, Phys. Rev. B **55**, 12748 (1997).
- ²⁰ O. K. Andersen, O. Jepsen, A. I. Liechtenstein, and I. I. Mazin, Phys. Rev. B **49**, 4145 (1994); J. Phys. Chem. Solids **56**, 1573 (1995).
- ²¹ M. Opel, R. Nemetschek, C. Hoffmann, R. Philipp, P. F. Müller, R. Hackl, I. Tüttö, A. Erb, B. Revaz, E. Walker, H. Berger and L. Forró, Phys. Rev. B **61**, 9752 (2000).
- ²² F. Venturini, M. Opel, T. P. Devereaux, J. K. Freericks, I. Tüttö, B. Revaz, E. Walker, H. Berger, L. Forró, and R. Hackl, Phys. Rev. Lett. **89**, 107003 (2002).
- ²³ A. Hosseini, R. Harris, S. Kamal, P. Dosanjh, J. Preston, R. Liang, W. N. Hardy, and D. A. Bonn, Phys. Rev. B **60**, 1349 (1999).
- ²⁴ D. A. Bonn, R. Liang, T. M. Riseman, D. J. Baar, D. C. Morgan, K. Zhang, P. Dosanjh, T. L. Duty, A. MacFarlane, G. D. Morris, J. H. Brewer, W. N. Hardy, C. Kallin and A. J. Berlinsky, Phys. Rev. B **47**, 11314 (1993).
- ²⁵ P. J. Hirschfeld, S. M. Quinlan, and D. J. Scalapino, Phys. Rev. B **55**, 12742 (1997).
- ²⁶ P. J. Hirschfeld, W. O. Puttika, and D. J. Scalapino, Phys. Rev. Lett. **71**, 3705 (1993); Phys. Rev. B **50**, 10254 (1994).
- ²⁷ S. Hensen, G. Müller, C. T. Rieck and K. Scharnberg, Phys. Rev. B **56**, 6237 (1997).
- ²⁸ M. B. Walker and M. F. Smith, Phys. Rev. B **61**, 11285 (2000); D. Duffy, P. J. Hirschfeld, and D. J. Scalapino, **64**, 224522 (2001).
- ²⁹ M. Matsukawa, T. Mizukoshi, K. Noto, and Y. Shiohara, Phys. Rev. B **53**, 6034 (1996).
- ³⁰ A. Hosseini, S. Kamal, D. A. Bonn, R. Liang, and W. N. Hardy, Phys. Rev. Lett. **81**, 1298 (1998).
- ³¹ T. P. Devereaux and A. P. Kampf, Int. Journ. Mod. Phys. B **11**, 2093 (1997).
- ³² W. C. Wu and J. P. Carbotte, Phys. Rev. B **57**, 5614

(1998).

³³ B. S. Shastry and B. I. Shraiman, Phys. Rev. Lett. **65**, 1068 (1990); Int. Journ. Mod. Phys. B **5**, 365 (1991); A. Virosztek and J. Ruvalds, Phys. Rev. B **45**, 347 (1992).

³⁴ J. K. Freericks and T. P. Devereaux, Phys. Rev. B **64**, 125110 (2001); J. K. Freericks, T. P. Devereaux, and R. Bulla, Phys. Rev. B **64**, 233114 (2001).

³⁵ See, Z-X. Shen and J. R. Schrieffer, Phys. Rev. Lett. **78**, 1771 (1997) for example.

³⁶ S. V. Borisenko, A. A. Kordyuk, S. Legner, C. Dürr, M. Knupfer, M. S. Golden, J. Fink, K. Nenkov, D. Eckert, G. Yang, S. Abell, H. Berger, L. Forró, B. Liang, A. Maljuk, C. T. Lin, and B. Keimer, Phys. Rev. B **64**, 094513 (2001); P. V. Bogdanov, A. Lanzara, X. J. Zhou, S. A. Kellar, D. L. Feng, E. D. Lu, H. Eisaki, J.-I. Shimoyama, K. Kishio, Z. Hussain, and Z. X. Shen; *ibid*, 180505 (2001).

³⁷ A. C. Durst and P. A. Lee, Phys. Rev. B **62**, 1270 (2000).

³⁸ T. P. Devereaux and A. P. Kampf, Phys. Rev. B **59**, 6411 (1999).

³⁹ More generally, in off-resonance conditions the vertices can be classified by symmetry in terms of BZ or FS harmonics.

⁴⁰ D. Poilblanc, D. J. Scalapino, and W. Hanke, Phys. Rev. Lett. **72**, 884 (1994); A. P. Kampf and T. P. Devereaux, Phys. Rev. B **56**, 2360 (1997).

⁴¹ F. Venturini, Q.-M. Zhang, R. Hackl, A. Lucarelli, S. Lupi, M. Ortolani, P. Calvani, N. Kikugawa, and T. Fujita, Phys. Rev. B **66**, 060502 (2002); private communication.

⁴² S. A. Kivelson, E. Fradkin, and V. J. Emery, Nature **39**, 550 (1998); E. W. Carlson, V. J. Emery, S. A. Kivelson, and D. Orgad, cond-mat/0206217.

⁴³ L. B. Ioffe and A. J. Millis, cond-mat/0112509.

⁴⁴ T. P. Devereaux and A. P. Kampf, Phys. Rev. B **61**, 1490 (2000).

⁴⁵ M. Chiao, R. W. Hill, C. Lupien, L. Taillefer, P. Lambert, R. Gagnon, and P. Fournier, Phys. Rev. B **62**, 3554 (2000).

⁴⁶ T. P. Devereaux, A. Virosztek and A. Zawadowski, Phys. Rev. B **54**, 12523 (1996); T. P. Devereaux and D. Einzel, **51**, 16336 (1995).

⁴⁷ This treatment does not consider the interplay of disorder and interactions (and particular misses out on the physics of the Anderson-Mott transition) and can only be considered this way in the limit of weak scattering. Efforts to include both disorder and interactions equally in a T-matrix approach have been put forward, most recently in Ref.⁴⁴.

⁴⁸ M. J. Graf, S.-K. Yip, J. A. Sauls, and D. Rainer, Phys. Rev. B **53**, 15147 (1996).

⁴⁹ M. J. Graf, M. Palumbo, D. Rainer, and J. A. Sauls, Phys. Rev. B **52**, 10588 (1995).

⁵⁰ Y. I. Latyshev, T. Yamashita, L. N. Bulaevskii, M. J. Graf, A. V. Balatsky, and M. P. Maley, Phys. Rev. Lett. **82**, 5345 (1999).

⁵¹ S. Quinlan, D. J. Scalapino, and N. Bulut, Phys. Rev. B **49**, 1470 (1994).

⁵² S. M. Quinlan, P. J. Hirschfeld, and D. J. Scalapino, Phys. Rev. B **53**, 8575 (1996).

⁵³ B. S. Shastry, Phys. Rev. Lett. **63**, 1288 (1989); D. C. Mattis, Phys. Rev. Lett. **74**, 3676 (1995).

⁵⁴ J. H. Jefferson, H. Eskes, and L. F. Feiner, Phys. Rev. B **45**, 7959 (1992).